Int. J. Electrochem. Sci., 13 **(2018)** 4792 – 4807, doi: 10.20964/2018.05.79

International Journal of
ELECTROCHEMICAL
SCIENCE
www.electrochemsci.org

Electropolishing Mechanism of Ti-6Al-4V Alloy Fabricated by Selective Laser Melting

Yifei ZHANG, Jianzhong LI[*], *Shuanghang CHE*

School of Metallurgy, Northeastern University, Shenyang city, 110819, China
[*]E-mail: lijz@smm.neu.edu.cn

Received: 21 January 2018 / *Accepted:* 16 March 2018 / *Published:* 10 April 2018

In this study, the electropolishing mechanism of Ti-6Al-4V alloy fabricated by selective laser melting was analysed by using the electrolyte of perchloric acid and glacial acetic acid. The influences of electropolishing time on the surface morphology and corrosion performance of the Ti-6Al-4Al alloy were investigated, with regard to the surface morphology, chemical compositions and corrosion behaviours, using scanning electron microscopy, atomic force microscopy, X-ray photoelectron spectroscopy, potentiodynamic polarization and electrochemical impedance spectroscopy. The results show that after electrochemical polishing, the surface of the Ti-6Al-4V alloy was covered with a thin layer of oxide film composed of titanium, aluminium and vanadium oxides. The surface roughness of the Ti-6Al-4V alloy with an electropolishing time of 15 min was at its minimum, reaching an ideal polishing effect. The electropolishing mechanism of the Ti-6Al-4V alloy was the shedding of spherical particles on the alloy surface and the smoothing of prominent parts under the electrochemical reaction. As the electropolishing time increased, the corrosion resistance of the Ti-6Al-4V alloy in Ringer's solution initially increased then decreased. The increment in VO_x content and oxidation of unstable and low-valence TiO, or Ti_2O_3 into stable and compact TiO_2 in the oxide film triggered by prolonging polishing time were found to enhance corrosion resistance.

Keywords: Ti-6Al-4V alloy; Electrochemical polishing; Surface morphology; Oxide film; Corrosion performance

1. INTRODUCTION

As a moderate strength titanium alloy with a microstructure of α+β two-phase, Ti-6Al-4V (TC4) alloy has been widely used in human implants, biomedical engineering and other fields because of its superior corrosion resistance, small density, high specific strength, favourable toughness and good biocompatibility [1,2]. In these fields, however, machining deformation always occurs when manufacturing titanium alloys by using traditional methods, making it difficult to meet its application requirements [3]. To solve this problem, Ti alloys prepared by selective laser melting (SLM) have

become a research hotspot in recent years. SLM technology is based on a digital model file, and it uses powdery metal or plastic and other adhesive materials to manufacture an object layer by layer [4,5]. Owing to its excellent mechanical characteristics, chemical properties and processing performance, titanium alloy has become an important material in SLM technology. Research on the technology, microstructures, heat treatment and mechanical properties of Ti-6Al-4V alloy fabricated by SLM is widespread [6], and its results have supported the growth in the application development of selective laser-melted titanium alloys [7,8].

Nevertheless, because of an unsuitable energy density in the manufacturing process, components of titanium alloys fabricated by SLM tend to produce pores and unmelted powder defects, leading to a drop in surface smoothness and thus performance [9]. To enhance the surface state of titanium alloys prepared by SLM, surface treatments have often considered using mechanical, chemical and electrochemical methods to obtain a smooth surface [10]. Among these, one effective treatment method is electrochemical polishing. This method can fabricate titanium alloys free of stress and occlusions, most of which have a microscopically smooth surface or even a "mirror" effect [11]. Furthermore, the complex shape of the polished part may be created by a flexible power line and flow electrolyte, ensuring that the corrosion resistance of the polished alloys is enhanced and the parts' surfaces cleaned by microorganisms. Further, no deformation occurs on the electropolished alloy surface and the alloy maintains its original lattice structure [12,13]. Yang [14] pointed out that the electropolishing process has the potential to improve the mechanical properties of the Ti-6Al-4V parts produced by an additive manufacturing process. Aderico [15] studied the surface roughness and fatigue performance of Ti-6Al-4V alloy after different polishing methods and found that the specimen after electrolytic polishing was more effective than that after conventional polishing; moreover, the surface roughness did not affect fatigue performance. Urlea [16] optimized the current density for efficient electrochemical polishing of Ti-6Al-4V components. Kiyoshi [17] developed a new electropolishing system composed of alcohol for wrought CP titanium and titanium alloys. He found that the SEM images of CP Ti were uniform and completely free of features, whereas the TC4 alloy appeared pitted. However, the research samples of previous studies have been confined only to traditional titanium alloys.

Although many previous investigations have reported the properties and electrochemical behaviours of traditional titanium alloys after electropolishing based on different bath components and process parameters, the special surface state of selective laser-melted titanium alloys has limited their usage [18]. This can be ascribed to the reason that the titanium alloys fabricated by SLM often have an incomplete melting powder, which generates an oxide film-like ceramic with high hardness and low chemical activity [19]. Meanwhile, some SLM-produced alloys contain micron-sized pores, microcracks and other defects due to the entrapment of gases or inappropriate fusion between successive tracks or layers [20]. In this paper, the surface treatment of TC4 alloy fabricated by SLM was conducted by using an electropolishing method to investigate the effects of electropolishing time on surface compositions; then, the electropolishing mechanism of TC4 alloy was also analysed systematically. Electrolyte composition was determined by running a factor experiment.

In addition, act as tissue substitutes or in vivo implants, the corrosion resistance and biocompatibility of polished TC4 alloys must be detected and enhanced [21]. Despite research efforts

to develop corrosion mechanisms for titanium alloys, limited data taking in simulated body fluid are available to evaluate the corrosion behaviours of electropolished titanium alloys fabricated by SLM. Therefore, in this strand of the literature, the corrosion performance of samples in different polishing stages has also been analysed by using simulated body fluid (Ringer's solution) to optimize the electrolysis process and improve the corrosion resistance and biocompatibility of Ti-6Al-4V alloy.

2. EXPERIMENTAL

2.1 Materials

Spherical powder of Ti-6Al-4V (Grade 23) obtained from the Shanghai Research Institute of Materials was used for SLM. The size range of the powder was 20~30 μm and the apparent density was 2.5 g/cm^3. SLM experiments were performed under the same process conditions, using EOSINT M270 equipment manufactured by EOS (Germany). Under the direction of the hierarchical structures of 3D CAD models, the samples were produced layer-by-layer in the horizontal direction. The chemical composition of the Ti-6Al-4V alloy produced and analysed in this research is listed in Table 1.

Table 1. Chemical composition of Ti-6Al-4V alloy

element	N	C	Fe	H	Al	V	O	Ti
Wt/%	0.05	0.01	0.3	0.015	6.2	4.5	0.2	Balance

2.2 Electrochemical polishing

Before electrochemical polishing, the Ti-6Al-4V alloys were initially cleaned for 5 min in an ultrasonic wash in alcohol electrolyte. Then, the samples were electropolished in a bath solution of perchloric acid and glacial acetic acid. Based on the simultaneous change in sample weight and surface roughness, the electrolyte composition, temperature and current density were determined. The electrolytic solution contained perchloric acid, glacial acetic acid and distilled water with a volume ratio of 1:10:1.2. The electrolytic polishing conditions were as follows: current density was 0.3 A/cm^2, polishing temperature was 30℃ and the space between the electrodes was 5 cm. Then, four groups of samples were polished electrochemically for 5, 10, 15 and 20 min.

2.3 Surface analysis

The mean roughness factor Ra and weight loss of the Ti-6Al-4V alloys were measured by using a Mahr profilometer and FA1004 electronic scales, respectively. The morphology characterization of the sample surface after electropolishing for the different times was studied by using the Quanta FEG 250 scanning electron microscope and NanoScope E atomic forces microscope.

The compositions of the oxide film that had formed on the alloy surface after the electropolishing process were detected by using a Thermo Scientific Escalab 250Xi Photoelectron Spectrometer (XPS). Photoelectron emission was excited by a monochromatic Al K_α source with a powder of 150 W and an initial photo energy of 1486.6 eV. A peak of the contaminative carbon of 284.8 eV was used as a reference for correcting the charge shifts. Then, the chemical state speciation of Ti, Al, V, Fe, N, O, Cl and so forth on the oxide film of the alloy surface was conducted by using XPS peak41 software.

2.4 Electrochemical measurements

The specimens (20×20×2 mm) with different electrochemical polishing times were prepared for the electrochemistry experiment. Before all measurements, the specimens after electrochemical polishing were ground by using silicon carbide papers in a 1200 mesh and ultrasonically cleaned in an ethanol bath for 5 min; they were then rinsed with distilled water. To estimate the corrosion behaviour of the TC4 alloy after electropolishing in simulated body fluids, all tests were conducted in Ringer's solution (8.6 g/L NaCl -0.3 g/L KCl -0.33 g/L $CaCl_2 \cdot 2H_2O$). Electrochemical measurements were performed by using an electrolytic cell with a three-electrode configuration. A standard calomel electrode (SCE) was used as a reference and a graphite electrode as a counter electrode. The exposed area of the titanium alloy sample was approximately 1 cm^2. Before taking the potentiodynamic measurements, the open circuit potential was left stabilizing for 60 min. Then, potentiodynamic polarization was obtained from -1.0 V to 1.5 V (vs. SCE) at a scan rate of 5 mV/s. Electrochemical impedance spectroscopy (EIS) experiments were conducted by using a model PARSTAT 2273 (American Princeton Company) electrochemical workstation. Impedance measurements were performed from 10^{-2} to 10^5 Hz with an amplitude of 10 mV. The impedance spectra data were analysed by using ZSimpWin software and equivalent circuit models were simulated to evaluate the corrosion characteristics of the alloy samples.

3. RESULTS AND DISCUSSION

3.1 Surface analysis

3.1.1 Surface morphology

Table 2 presents the surface roughness and weight loss of the Ti-6Al-4V alloys during for the different electropolishing times. The surface morphology of the samples during electrolytic polishing is shown in Fig. 1.

Table 2. Surface roughness and weight loss of the Ti-6Al-4V alloys after electropolishing

Sample No.	0	1	2	3	4
Polishing time (min)	0	5	10	15	20
Roughness (Ra/μm)	6.33	2.01	1.63	1.132	1.72
Weight loss (%)	--	5.98	10.82	14.76	16.29

Note: No.0 is the original sample without electrochemical polishing.

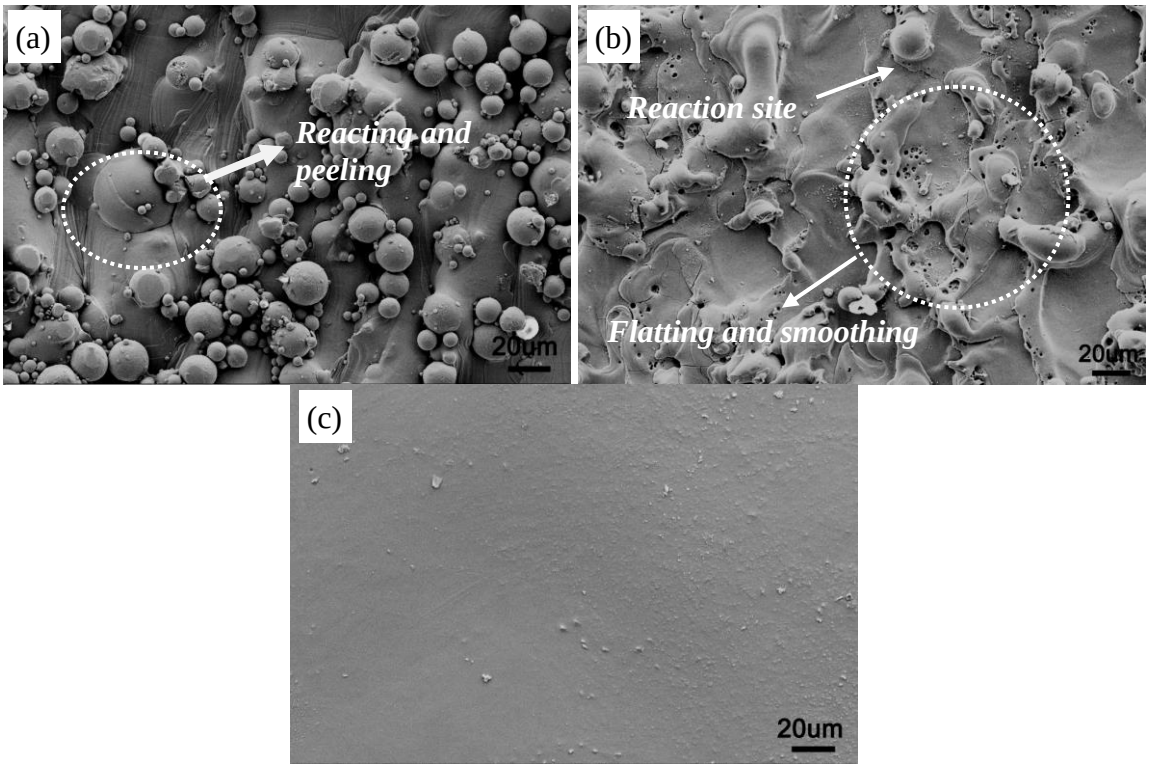

Figure 1. Surface morphology of the Ti-6Al-4V alloy during the electropolishing process (a) before electropolishing (b) electropolishing for 5 min (c) electropolishing for 15 min

As shown in Table 2 and Fig. 1, the surface roughness of the samples after electropolishing reduced and the weight decreased. Sample 3, with an electropolishing time of 15 min, had a better surface quality and the obtained surface was comparatively smooth and uniform. When the electropolishing time was less than 15 min, the surface roughness exhibited degressive trends; however, when the electropolishing time exceeded 15 min, the roughness showed a rising trend. Hence, under too short an electropolishing time, the sample surface cannot fully react and the surface removal is incomplete, resulting in a decrease in roughness. When the polishing time was 15 min, the sample surface reached a favourable polishing quality and the roughness was minimized. As the electropolishing time increased, small pits appeared on the sample surface in response to the excessive corrosion time, which in turn resulted in an increase in surface roughness and lower polishing quality.

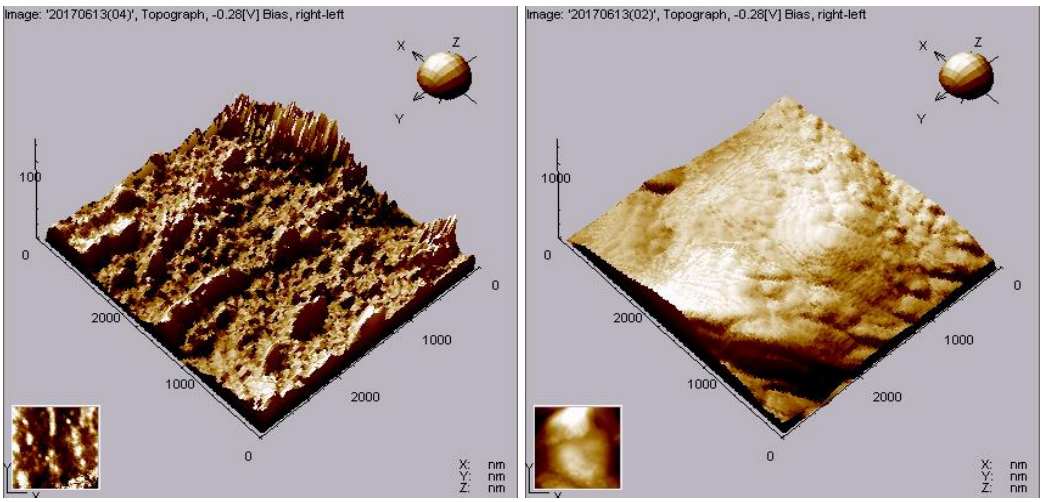

Figure 2. AFM images of the Ti-6Al-4V alloy surface after different electropolishing times (a) electropolishing for 5min (b) electeopolishing for 15 min

To observe the surface morphology of the polished Ti-6Al-4V alloy, an atomic force microscope (AFM) was used. The AFM images of the Ti-6Al-4V alloys after different electropolishing times are presented in Fig. 2. For the image with a 3×3 μm area shown in Fig. 2, the values of the macroscopic roughness index of the samples changed with different electropolishing times. For example, after electropolishing, the mean roughness index diminished from 6.33 μm (unpolished sample) to 1.13 μm (electropolishing for 15 min). The obtained alloy surface with 15 min electropolishing was more lustrous and uniform in all cases. The mean height of this sample calculated based on the AFM measurement was 243.81 nm and the maximum peak to valley (Rp-v) was 686.45 nm. This result also complements the roughness results listed in Table 2.

3.1.2 XPS analysis

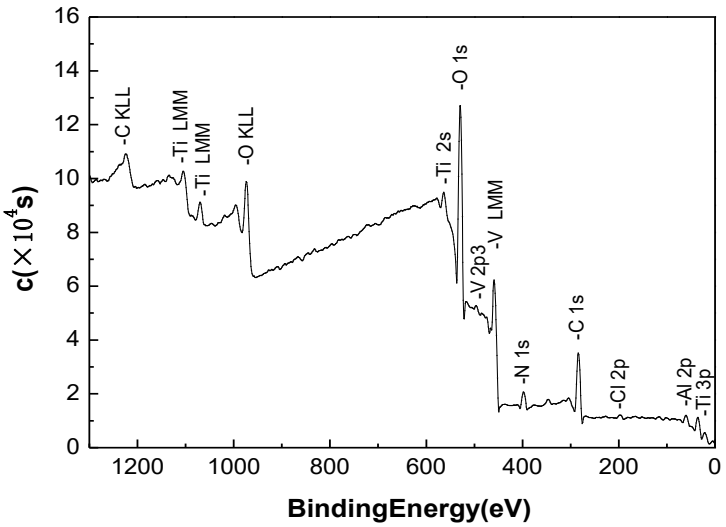

Figure 3. XPS spectra of the Ti-6Al-4V alloy surface after electropolishing for 20min

After electropolishing, an oxide layer generated spontaneously on the surface of the Ti-6Al-4V alloy in contact with the oxygen or acid solution. The composition and thickness of the oxide layer on the alloy surface are directly related to the electropolishing time, surface condition of the alloys and corrosion resistance of the elements.

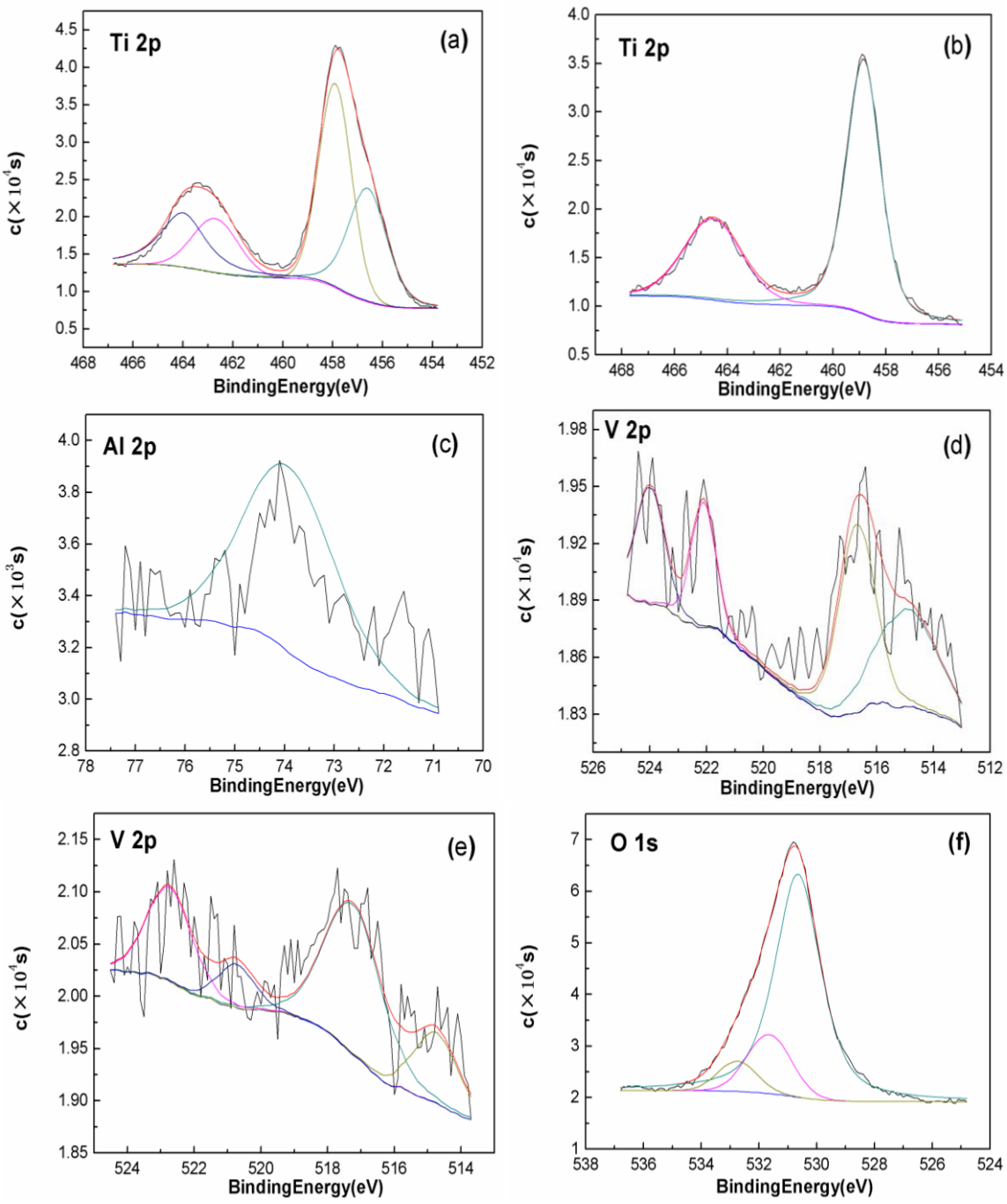

Figure 4. XPS spectra of Ti2p, Al2p, V2p, and O1s of the oxide films on the Ti-6Al-4V alloy surface with different electropolishing times(a) Ti2p spectra of alloy surface after 5min electropolishing (b) Ti2p spectra of alloy surface after 15min electropolishing (c) Al2p spectra of alloy surface after 5min electropolishing (d) V2p spectra of alloy surface after 10min electropolishing (e) V2p spectra of alloy surface after 15min electropolishing (f) O1s spectra of alloy surface after 15min electropolishing

The XPS of the Ti-6Al-4V alloy after electrochemical polishing is shown in Fig. 3, illustrating that many elements (Ti2p, Al2p, V2p, O1s, C1s, N1s, Fe2p and Cl2p) were detected on the alloy surface. By analysing the peak values of the XPS emission lines and binding energy of each element, it can be concluded that the thin layer of oxide film on the surface of the Ti-6Al-4V alloy after the electropolishing process was mainly composed of titanium, aluminium and vanadium oxides.

After 5 min electrochemical polishing, the oxides on the alloy surface were mainly composed of titanium oxide and aluminium oxide; almost no vanadium oxide was detected since the chemical properties of vanadium are stable and it is not easy to be oxidized during electropolishing. After electropolishing for 5 min, the titanium on the oxide film existed in the form of TiO and Ti_2O_3 (ca. 456.45 eV for TiO and 457.89 eV for Ti_2O_3), which were unstable and had no resistance to corrosion, as shown in Fig. 4(a). The peak at the binding energy of 74.04 eV (Al2p3/2) showed the presence of Al_2O_3 in the oxide film (Fig. 4(c)). Prolonging the electropolishing time intensified the oxidation reaction. After electropolishing for 10 min, vanadium oxide appeared, but the peak shape of vanadium was unclear, indicating that the content of vanadium oxide was lower. The peaks of vanadium were mainly concentrated between 514.31 and 515.67 eV (Fig. 4(d)). The relative content of the Ti:Al:V ratio in the oxide layer was 0.784:0.187:0.029. When the electropolishing time was extended to 15 min, accompanied by the grain growth, TiO and Ti_2O_3 were oxidized to anatase TiO_2 (metastable phase) and rutile TiO_2 (steady state), which were stable and had protective properties [22]. This fitted with the peaks in Fig. 4(b).

In the case of the vanadium spectrum, the binding energy of vanadium increased slightly, indicating that the valence of vanadium rises slightly and that the oxidation reaction of vanadium intensifies. The content of vanadium oxide in the film increased and the relative content of the Ti:Al:V ratio in the oxide layer was 0.743:0.221:0.036. The oxide layer generated on the alloy surface mainly consisted of TiO_2, Al_2O_3 and vanadium oxide (VO_X); the VO_X dominantly existed in the form of V_2O_3 (515.10 eV) and V_2O_4 (516.45 eV) (Fig. 4(e)).

In the oxygen spectrum, the peaks fit in the following forms: metallic oxide (530.65 eV), hydroxy (-OH, peak at 531.65 eV) and absorbed water (532.75 eV) (Fig. 4(f)). When extending the electropolishing time, similar compositions could be observed in the oxide layer. However, with the extension of the electropolishing time, over-corrosion appeared; further, some voids and other defects generated on the oxide film, leading to the deterioration of its stability.

Compared with the native oxide film composed of TiO_2 and Al_2O_3 formed in air, the main components of the oxide film after electropolishing were similar but vanadium oxide appeared and the structure of the oxide film differed. In the natural state, the oxidation of metals in the alloy surface followed the order of metal activity, i.e. Ti was oxidized preferentially and then Al (vanadium cannot be oxidized in air). Therefore, the oxide film covering the Ti-6Al-4V alloy exhibited a loose structure and thinner thickness. However, during the electropolishing process, the formed oxide film was more compact and thicker because of the simultaneous oxidization of Ti, Al and V under electrochemical action. Moreover, the produced higher valance oxides were more stable, which enhanced the corrosion resistance of the Ti-6Al-4V alloy immensely.

3.2 Electropolishing mechanism

As for the SLM-built titanium alloy, with the molten pool sunk into the supporting powder triggered by gravity and capillary forces, a mass of particles was attached to the overhanging surfaces, resulting in an inferior quality of the protuberate surface [23]. Given that the severe limitations of conventional mechanical and chemical polishing means finishing internal cavities and eliminating surface characteristics, electropolishing technology is regarded as one of the most appropriate methods for improving the surface quality of SLM-built alloys [24].

The electropolishing of the Ti-6Al-4V alloy in the solution of perchloric acid and glacial acetic acid system had three stages. In the first stage, the oxidation of the metals on the alloy surface proceeded, and the following reactions were obtained (VOx represents vanadium oxide such as V_2O_3, V_2O_4, and V_2O_5, as this is difficult to form in the natural state):

$$Ti + O_2 = TiO_2 \quad (1)$$

$$4Al + 3O_2 = 2Al_2O_3 \quad (2)$$

$$2V + xO_2 = 2VO_x \quad (3)$$

And

$$Ti + 2H_2O = TiO_2 + 4H^+ + 4e \quad (4)$$

$$2Al + 3H_2O = 2Al_2O_3 + 6H^+ + 6e \quad (5)$$

$$V + xH_2O = VOx + 2xH^+ + 2xe \quad (6)$$

In the second stage, the formed surface oxides reacted with the perchloric acid in the electrolyte and the oxides dissolved simultaneously as electropolishing progresses according to the reactions as follows:

$$Al_2O_3 + 6H^+ = 2Al^{3+} + 3H_2O \quad (7)$$

$$TiO_2 + 4H^+ = Ti^{4+} + 2H_2O \quad (8)$$

$$VO_x + 2xH^+ = V^{2x+} + xH_2O \quad (9)$$

The third stage is the macro-/micro-smoothing of the alloy surface. With the electropolishing progress, the alloy surface is constantly levelled and smoothed after the oxide desquamate in the form of large particles.

During electrochemical polishing, perchloric acid is the main reactant that reacts with the Ti-6Al-4V alloy; the glacial acetic acid in the electrolyte also plays a crucial role in the catalytic oxidation. In addition, the incomplete ionization of perchloric acid in glacial acetic acid ensures the safety of the reaction environment. During the electropolishing process, the oxidation reaction and polishing reaction mentioned above were always carried out simultaneously in the cell. When the polishing reaction dissolved the titanium atoms from anode, the oxidation reaction formed a thin oxide layer on the surface of the alloy, thereby inhibiting the diffusion of titanium anion into the electrolyte.

The model of the electropolishing mechanism of the Ti-6Al-4V alloy is presented in Fig. 5. Analysing the electropolishing mechanism shows that the protruding positions on the surface of the TC4 alloy fabricated by SLM easily react to the oxygen and produce spherical oxide particles (Fig. 5(a)). During the electropolishing process, the electrolytes concentrated in the sunken part, which connects the alloy base and the oxide particles, are in the majority; hence, the electrochemical reaction

primarily tends to occur here (see Fig. 1(b)), leading to the erosion and dissolution of the oxides. Due to the large cohesive force inside the oxides, the particles peeled gradually as a whole; therefore, the weight loss of samples during this period was the highest (Fig. 5(b)).

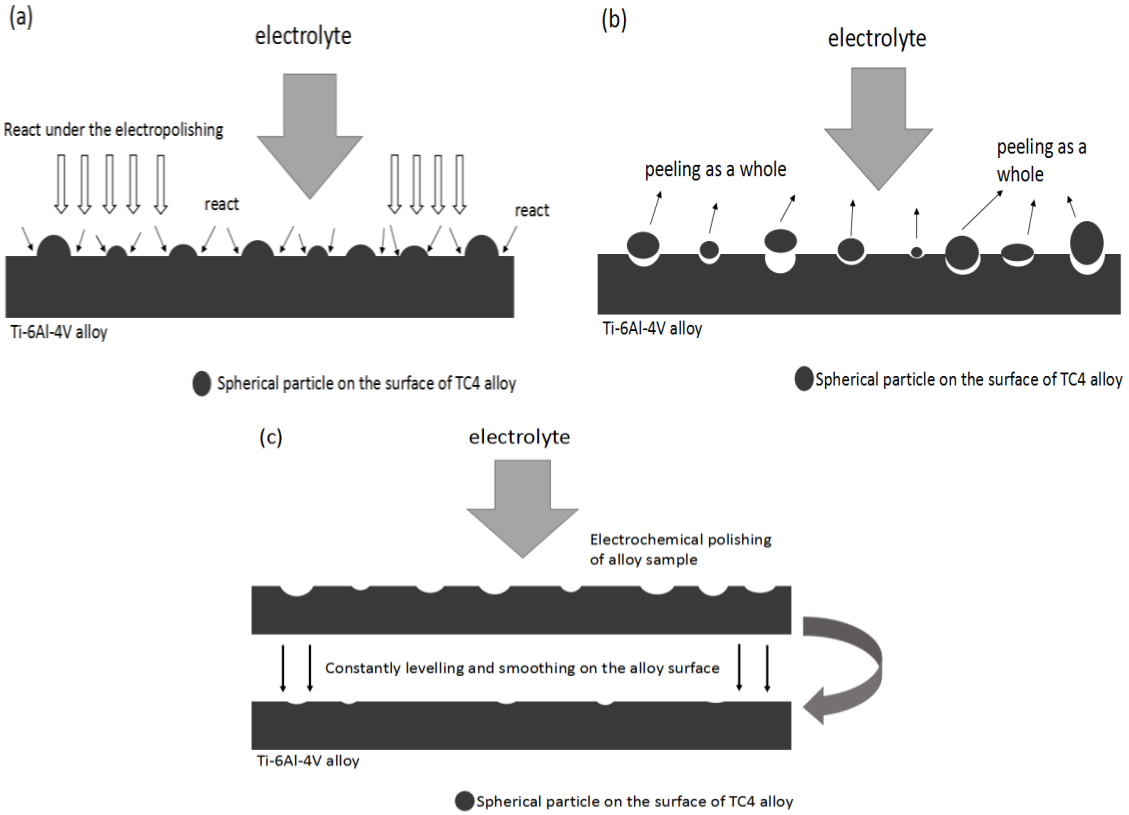

Figure 5. Mechanism of electropolishing of the Ti-6Al-4V alloy

Afterwards, the relatively prominent parts of the alloy surface began to react, the surface roughness of the Ti-6Al-4V alloy reduced constantly and the weight decreased gradually, reaching a smooth and lustrous surface (Fig. 5c)). This is consistent with the SEM results of the surface morphology of the Ti-6Al-4V alloy with different electropolishing times (see Fig. 1).

3.3 Electrochemical performance

3.3.1 Potentiodynamic polarization curves

The potentiodynamic polarization curves of the Ti-6Al-4V alloys after electropolishing in Ringer's solution are shown in Fig. 6. To facilitate the analysis, the corresponding data obtained from the polarization curves are tabulated in Table 3. The corrosion current density is expressed as I_{corr}, the corrosion potential is denoted by E_{corr} and I_{pass} is the passive current density.

Table 3. Electrochemical parameters of the Ti-6Al-4V alloys after polishing for different times

Sample No.	Polishing time (min)	Parameters		
		I_{corr} (uA/cm^2)	E_{corr} (V)	I_{pass} (uA/cm^2)
1	5	0.26	-0.67	2.02
2	10	0.20	-0.60	3.11
3	15	0.22	-0.58	1.80
4	20	0.46	-0.58	3.84

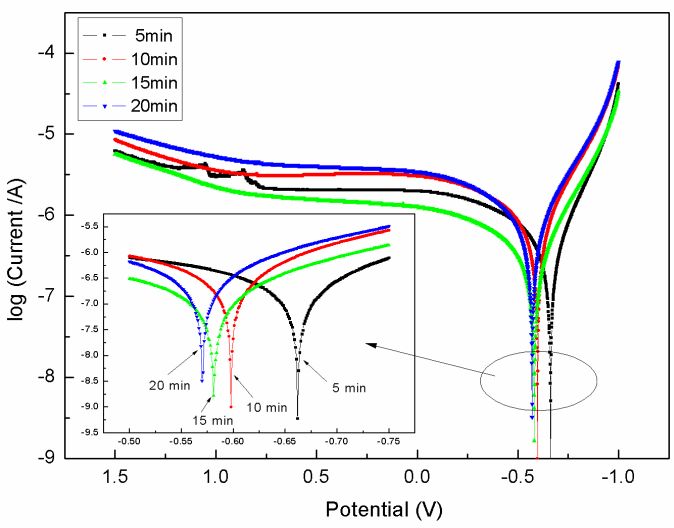

Figure 6. Polarization curves of the Ti-6Al-4V alloys after different electropolishing times

On the anodic branches, the current density of the Ti-6Al-4V alloy increased with the potential increasing from the open circuit potential to 0 V/SCE, and then changed little in the region from 0 V to 0.75 V, which portended the Ti-6Al-4V alloy staying in a passivation process. After electrochemical polishing, the corrosion potential gradually increased, meaning that the corrosion tendency of samples weakened and corrosion resistance enhanced. After electropolishing for 5 min, the corrosion potential (E_{corr}) of the alloy was the smallest; hence, by increasing the electropolishing time, the E_{corr} of samples gradually rose. There was no obvious difference between the polarization curves of the polished samples for 10 and 20 min. This finding illustrates that the corrosion resistance and passive film stability of the Ti-6Al-4V alloy with electropolishing for 10 min was comparable to that of electropolishing for 20 min. For the Ti-6Al-4V alloy, for electropolishing for 15 min, the corrosion potential was higher and the passive current density was lower, indicating that the corrosion tendency of this sample weakened. Hence, it was easy to enter a passivation state, exhibiting better corrosion resistance. Moreover, a higher passive current density (I_{pass}) with electropolishing for 20 min was also observed, which may have caused the formation of defects in the oxide film (i.e. there was a tendency to form a more irregular or porous oxide layer).

According to Faraday's law, $Q=m\bullet F$, Q indicates the quantity of electricity passing through the electrode, m represents the amount of a substance in the corresponding chemical changes, and F is Faraday's constant. It can be deduced that $V=(M\bullet i)/F$, where i indicates the anode current through the

unit area of the anode region, *V* represents the average velocity of the metal mass loss in the unit area of the anode region, and *M* is the relative molecular mass or the relative atomic mass of metals [25,26]. Therefore, the self-corrosion current density is proportional to the corrosion rate and Icorr can be used as an index to reflect the speed of electrode corrosion. As presented in Table 3, compared with the sample with an electropolishing time of 20 min, the corrosion rate of the sample with an electropolishing time of 10 min was much lower, indicating that the corrosion resistance of the sample with an electropolishing time of 10 min was slightly stronger than that of electropolishing for 20 min.

3.3.2 EIS measurements

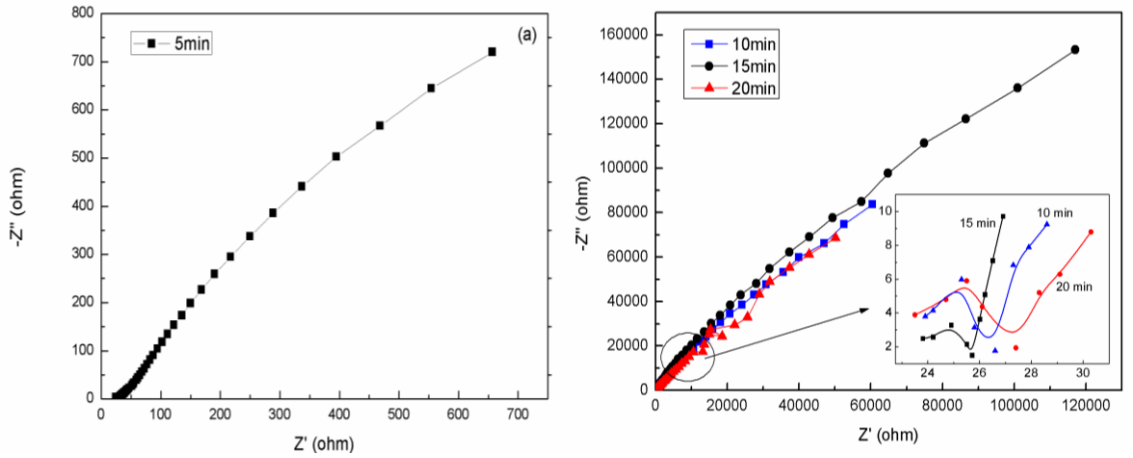

Figure 7. Nyquist plots of the Ti-6Al-4V alloys with different electropolishing times

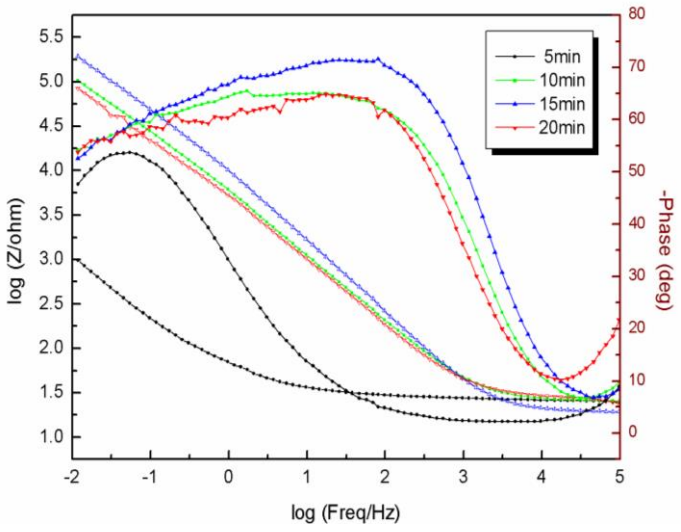

Figure 8. Bode diagrams of the Ti-6Al-4V alloys at different electropolishing times

EIS testing is an effective means of determining the corrosion resistance of titanium alloys. Nyquist and Bode plots for the Ti-6Al-4V alloys at different electropolishing times are presented in Fig. 7 and Fig. 8. As shown in Fig. 7, in the sample with an electropolishing time of 5 min, only one

capacitive arc appeared compared with two capacitive arcs generated when extending the electropolishing time to 10 min or more. Compared with the Nyquist plots, the Bode diagrams are more characteristic and better show the changes in the electrochemical characteristics at different electropolishing times.

Fig. 8 presents the Bode diagrams obtained before polarization for the alloy samples in Ringer's solution. The slow diffusion of O through the barrier layer restricted the total corrosion rate of the alloys in Ringer's solution. Assume that the high |Z| at low frequencies in Fig. 8 reflects the degree of the diffusion of O through the barrier layer into the TC4 alloy matrix. The low-frequency arc in this figure reveals the resistance of the barrier layer [28]. An increase in |Z| can be observed in the low-frequency region when raising the electropolishing time from 5 min to 15 min, implying a reduction in corrosion degree. Moreover, when extending the electropolishing time to 20 min, over-etching appeared, which in turn resulted in an increase in corrosion degree.

Resistance at high frequencies (10^4–10^5 Hz) corresponded to the solution resistance. The modulus diagram at high frequencies was a horizontal shape, indicating that the solution resistance was a dominant factor responsible for the impedance [29]. The phase-frequency characteristic curve in Fig. 8 shows that when the electropolishing was 5 min, the electrochemical reaction was slower. Increasing the electropolishing time to 10 min accelerated the electrochemical reaction. Continuing to increase the electropolishing time changed the reaction rate little, and the sample gradually entered the passivation region. The sample with an electropolishing time of 15 min had the largest phase angle, indicating that the passivation film of this sample was more complete and the corrosion resistance was better. Moreover, displacement at phase angles under different electropolishing times was also presented. Such displacement was more distinct for samples at a middle frequency from 10^1 to 10^2 Hz, while for samples with an electropolishing time of 10 or 20 min, this displacement was not apparent and the shapes of the curves were similar. The Bode diagrams of these two samples do not show significant alterations with an extension of the electropolishing time. The minus phase angle graph in Fig. 8 manifests a minimum phase angle in the frequency of 10^4–10^5 Hz, which separates the low and medium-frequency process from the high-frequency process. The low-frequency process is associated with the electron transfer of the barrier layer, while the high-frequency process involves the transportation situation of the substance at the interface. This distinction is generally considered to be the response of a non-homogeneous film containing a compact inner layer (commonly referred to as a barrier layer) and a porous outer layer [30].

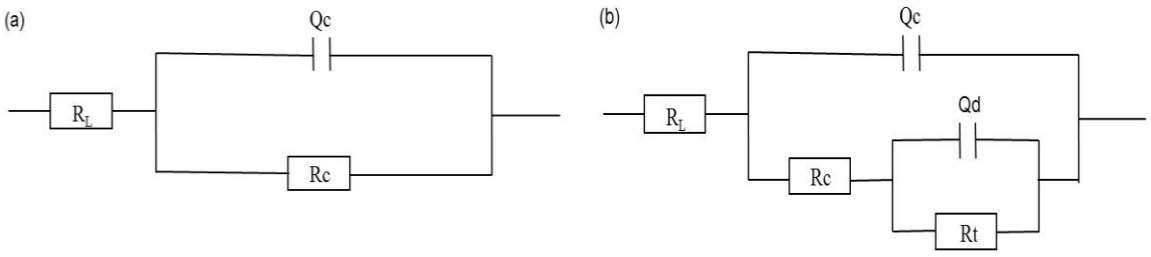

Figure 9. Equivalent electrical circuits used to adjust the EIS results (a) circuit 1 (b) circuit 2

The impedance data are fitted with the equivalent circuit by using ZSimpWin software, as shown in Fig. 9. RL is the solution resistance, and the circuit assumes that the oxide layer consists of an outer porous layer and an inner compact layer. Capacitance Q_C and resistance R_C correspond to the outer layer, while Qd and Rt relate to the capacitance and resistance of the inner compact layer, respectively. The specific fitting values are illustrated in Table 4.

Table 4. Impedance parameters of the Ti-6Al-4V alloys at different electropolishing times

Sample No.	polishing time (min)	R_L ($\Omega \cdot cm^2$)	Q_C ($F \cdot cm^{-2}$)	R_C ($\Omega \cdot cm^2$)	Q_d ($F \cdot cm^{-2}$)	R_t ($\Omega \cdot cm^2$)	Chi-squared (χ^2)
1	5	20.69	2.016e-2	758.40	--	--	2.02e-3
2	10	16.44	2.507e-5	8.56	2.663e-6	7.152e5	1.48e-3
3	15	21.49	5.625e-5	12.72	3.724e-6	1.014e6	7.97e-4
4	20	23.29	4.656e-5	23.56	2.051e-6	5.128e5	1.59e-3

Table 4 shows the fitting data results of the impedance parameters. The simulating error between the measured and calculated values was denoted by a chi-squared value (χ^2), and the results below 10^{-3} implied a preferable fitting effect. All the measuring results of the impedance parameters were adjusted with circuit 2, except for the sample of electropolishing for 5 min, which was adjusted with circuit 1.

From the fitting data above, it is observed that the passive film resistance and capacitance of sample polishing for 5 min were at least more than two orders of magnitude above those of the other samples, which implies that after polishing for 5 min, a compact or uniform passive film was generated on the alloy surface. The impedance spectrum of the oxide layer presented a single capacitive arc, indicating only one time constant. Moreover, extending the electropolishing time for all alloys presented two time constants. This demonstrates that as the electropolishing time increases, the oxide film on the titanium alloy surface appears as a bi-layer structure and the corrosion products penetrate the film structure and block the pores or other micro-defects in the oxide film, resulting in the reduction in Q_C capacitance and R_C resistance. R_C resistance, which largely relies on the amounts of pores and defects into which the solution can infiltrate, is a susceptive indicator of the existence of defects in an oxide film [31]. The parameters obtained by the impedance test illustrated that the resistance of the barrier layer is observably higher than the resistance related to the outer layer, indicating that the protective effect provided by the oxide film principally depends on the inner compact layer. The polarization resistances, defined as R_C+Rt, are concerned with the corrosion resistance of the alloy. As the electropolishing time prolongs, the polarization resistances firstly increase then decrease, showing the same tendency as the inner layer resistance. In particular, when the interface system or Rc is small or can be ignored, the properties of the oxide film on the alloy surface in Ringer's solution largely depend on the value of R_t.

Resistance Rc may be associated with the Helmholtz layer and thickness of the porous outer layer; resistance Rt with a large value links with the charge transfer and density of the barrier film [32]. The larger the resistance of the passivation film, the thicker is the passivation film; the larger the

charge transfer resistance, the smaller is the corrosion rate. These two factors are responsible for the corrosion reaction process. The compact inner layer, consisting of small or equiaxed grains of titanium, aluminium and vanadium oxides, appears to initiate in the region occupied by the alloy at the interface on the alloy matrix and could trigger high resistance (low-frequency arc). The porous outer layer composed of the titanium oxides, aluminium oxides, internal solution and Helmholtz layer may lead to relatively low resistance (high-frequency arc). As seen from the phase-frequency curves (Fig. 8), when the electropolishing time was 5 min, the wave crest of the minus phase angle in the low-frequency region was at its minimum. When increasing the electropolishing time, the peak of the wave moved in the high-frequency direction and the phase angle corresponding to the peak value became larger, indicating that the integrality of the passive film generated on the alloy surface was enhanced and the corrosion resistance of the titanium alloy improved. At an electropolishing time of 15 min, the Ti-6Al-4V alloy achieved a favourable corrosion resistance effect.

4. CONCLUSIONS

1) Electropolishing with a solution composed of perchloric acid and acetic acid achieves very good effects for the Ti-6Al-4V alloy. After the electropolishing process, the surface roughness of the Ti-6Al-4V alloy reduced markedly and the alloy obtained a lustrous surface. For an electropolishing time of 0 to 20 min, the surface roughness of the alloys with electropolishing of 15 min was smaller and the polishing effect improved.

2) The electropolishing mechanism of a Ti-6Al-4V alloy is the shedding of spherical particles on the alloy surface under an electrochemical reaction and the smoothing of prominent parts. After electropolishing, a thin oxide layer formed on the alloy surface spontaneously, while the compositions of the oxide film changed with different electropolishing times.

3) The oxide films consists of a mixture of titanium oxide (TiO_X), Al_2O_3 and vanadium oxide (VO_X). With an increasing electropolishing time, unstable and unprotective TiO and Ti_2O_3 are gradually oxidized to anatase TiO_2 or rutile TiO_2, which are denser and more stable. The content of vanadium in the oxide film increased and the valence elevated.

4) The corrosion resistance of the alloy is related to the electropolishing time. After the electropolishing process, the corrosion resistance of the Ti-6Al-4V alloy enhanced. During an electropolishing time of 0 to 20 min, the corrosion resistance of the Ti-6Al-4V alloy initially increased then decreased. The Ti-6Al-4V alloy with a 15 min electropolishing time exhibited favourable corrosion resistance.

ACKNOWLEDGEMENTS
This work was supported by the National Natural Science Foundation of China [grant number 51374053] and the Iron and Steel Joint Research Found of National Natural Science Foundation and China Baowu Steel Group Corporation Limited [grant number U1760118].

References

1. S. Leuders, M. Thone, A. Riemer, T. Niendorf, T. Tröster, H.A. Richard and H.J. Maier, *Int J Fatigue*, 48 (2013) 300.

2. K. S. Chan, D. L. Davidson, Fatigue crack growth in fiber growth in fiber-reinforced metal-matrix composite, Fatigue of Advanced Materials, Materials and Component Engineering Publishing(MCEP), 1991, Birmingham, Unoted Kingdom.
3. S. Zhang, R.Z. Gui and Q.S. Wei and Y.S. Shi, J. *Mech. Eng*, 49 (2013) 21.
4. H. Attar, K.G. Prashanth, L.C. Zhang, M. Calin, I.V. Okulov, S. Scudino, C. Yang and J. Eckert, *J. Mater. Sci. Technol*, 31 (2015) 1001.
5. S. Romankov, Y. Hayasaka and N. Hayashi, *J. Alloys Compd*, 495 (2010) 625.
6. Z. Zhao, J. Chen, X.F. Lu, H. Tan, X. Lin and W.D. Huang, *Mater. Sci. Eng*., A, 691 (2017) 16.
7. S. D. Sun, Y.Y. Zong, D.B. Shan and B. Guo, *Trans. Nonfeerous Met. Soc. China*, 20 (2010) 2181.
8. G. M. Hoinard, W. Elmay, L. Peltier and P. Laheurte, *J. Mech. Behav. Biomed. Mater*, 71 (2017) 32.
9. G. Li, S.G. Qu and Y.X. Pan, *Appl. Surf. Sci*, 339 (2016) 324.
10. W. Simka, M. Mosiałek, G. Nawrat, P. Nowak, J. Żak, J. Szade, A. Winiarski, A. Maciej and L.S. Warszyńska, *Surf. Coat. Technol*, 213 (2012) 239.
11. C.W. Nahm, *Surf. Coat. Tech*, 233 (2013) 13.
12. S. Kumar, T.S N.S. Narayanan, S.G.S. Raman and S.K.Seshadri, M*ater. Chem. Phys*, 119 (2010) 337.
13. Z. Rahman, L. Pompa and W. Haider, *J. Mater Eng Perform*, 23 (2014) 3907.
14. A. Mohammad, M. K. Mohammed and A. M. Alahmari, *Int. J Adv Manuf Tech*, 87 (2016) 1033.
15. S. G. Aderico, A. Z. Ricardo, *J prosthet dent*, 93 (2005) 378.
16. V. Urlea, V. Brailovski, *J Mater Process Tech*, 242 (2017) 1.
17. K. Tajima, M. Hironaka, K.K. Chen, Y. Nagamatsu, H. Kakigawa and Y. Kozono, *Dent Mater J*, 27 (2008) 258.
18. P. Guo, Y. Zhao, W. Zeng and Q. Hong, *Mater. Sci. Eng*., A, 563 (2013) 106.
19. C. Velmurugan, V. Senthilkumar, S. Sarala and J. Arivarasan, *J. Mater. Process. Tech*, 234 (2016) 272.
20. B.J. Zhao, H. Wang, N. Qiao, C. Wang and M.Hu, *Mater. Sci. Eng. C*, 70 (2017) 832.
21. H. L. Liu, M. Niinomi, M. Nakai, K. Cho and H. Fujii, *Scripta Mater*, 130 (2017) 27.
22. N. Dai, L.C. Zhang, J.X. Zhang, X. Zhang, Q.Z. Ni, Y. Chen, M.L. Wu and C. Yang, *Corros. Sci*, 111 (2016) 703.
23. J. M. Williams, A. Adewunmi, R.M. Schek, C.L. Flanagan, P.H.Krebsbach, S. E.Feinberg, S. J. Hollister and S. Das, Biomaterials, 26 (2005) 4817.
24. C. C. Chen, J. H. Chen, C. G. Chao and C.S. Wen, *J. Mater Sci*, 40 (2005) 4053.
25. V. G. Pina, V. Amigó and A. I. Munoz, *Corros. Sci*, 109 (2016) 15.
26. M. E. Souza, L. Lima, C. R. Lima, C. A. Zavaglia and C.M. Freire, *J Mater Sci Mater Med*, 20 (2009) 549.
27. I. Cvijović-Alagić, Z. Cvijović, J. Bajat and M. Rakin, *Mater. Corros*, 67 (2016) 1075.
28. S. Wojciech, M. Michał, N. Ginter, P. Nowak, J. Zak, J. Szade, A. Winiarski, A. Maciej and L.S. Warszyńska, Surf. Coat. Technol, 213 (2012) 239.
29. V.Y. Zadorozhnyy, X. Shi, D.S. Kozak and D.V. Louzguine-Luzgin, *J. Alloys Compd*, 707 (2017) 291.
30. R. Sánchez-Tovar, R. Leiva-García and J. García-Antón, *Thin Solid Films*, 576 (2015) 1.
31. X.H. Liu, X.Q. Wu and E.H. Han, *Electrochim. Acta*, 108 (2013) 554.
32. S. Chakria, I. Frateura, M.E. Orazem, E.M.M.Sutter, T.T.M.Tran, B.Tribollet and V.Vivier, *Electrochim. Acta*, 246 (2017) 924.